

Scalable Formal Verification via Autoencoder Latent Space Abstraction

Robert Reed

Robert.Reed-1@colorado.edu
University of Colorado Boulder
Boulder, Colorado, USA

Luca Laurenti

L.Laurenti@tudelft.nl
Delft University of Technology
Delft, Netherlands

Morteza Lahijanian

Morteza.Lahijanian@colorado.edu
University of Colorado Boulder
Boulder, Colorado, USA

Abstract

Finite Abstraction methods provide a powerful formal framework for proving that systems satisfy their specifications. However, these techniques face scalability challenges for high-dimensional systems, as they rely on state-space discretization which grows exponentially with dimension. Learning-based approaches to dimensionality reduction, utilizing neural networks and autoencoders, have shown great potential to alleviate this problem. However, ensuring the correctness of the resulting verification results remains an open question. In this work, we provide a formal approach to reduce the dimensionality of systems via convex autoencoders and learn the dynamics in the latent space through a kernel-based method. We then construct a finite abstraction from the learned model in the latent space and guarantee that the abstraction contains the true behaviors of the original system. We show that the verification results in the latent space can be mapped back to the original system. Finally, we demonstrate the effectiveness of our approach on multiple systems, including a 26D system controlled by a neural network, showing significant scalability improvements without loss of rigor.

1 Introduction

Formal verification of continuous-space dynamical systems provides a rigorous way to guarantee that a system satisfies a desired specification [4, 29, 6]. A standard approach is to express the specification in Linear Temporal Logic (LTL) [4] and construct a finite-state abstraction that captures all possible behaviors of the system. Off-the-shelf model-checking tools can then be applied to this abstraction to determine whether the specification is satisfied. This approach, however, faces significant challenges when applied to *AI-enabled* systems, such as those controlled by neural networks that operate on *high-dimensional* sensor inputs (e.g., camera images or LiDAR). First, the size of the abstraction grows *exponentially with the dimension* of the state space. Second, for systems with *complex* or partially *unknown* dynamics, computing the transition relation between abstract states becomes highly nontrivial. Yet these challenges are increasingly critical, as AI components are rapidly becoming integral to modern autonomous systems. In this work, we aim to address these challenges by developing a formal verification framework for systems with unknown dynamics that scales to extremely high-dimensional settings.

Model order reduction has been widely used to simplify systems for classical control and verification [19, 5, 2]. However, for systems with highly complex or unknown dynamics, such reduction techniques often fail to generalize. To address this limitation, modern approaches employ data-driven techniques, such as autoencoders [7], to learn latent representations and latent dynamics

for control, typically trading correctness guarantees for flexibility. For systems with unknown dynamics, some works construct finite abstractions with correctness guarantees [27, 24], but these approaches suffer from scalability limitations. Applying such abstraction techniques directly in a learned latent space is challenging because existing frameworks assume explicit, well-defined system dynamics, whereas latent-space dynamics induced by learned representations may instead be governed by *inclusion* dynamics, violating these assumptions.

To the best of our knowledge, no existing method enables formal verification in a latent space against arbitrary LTL specifications *while also providing correctness guarantees* for both the mapping of specifications into the latent representation and the learned latent dynamics. This work bridges this gap by combining dimensionality reduction with abstraction-based verification to provide formal guarantees for high-dimensional systems with unknown dynamics. Our framework is built on two key observations: (i) the learned latent space must correctly represent the regions of interest in the state space, and (ii) the latent dynamics may naturally follow an inclusion model. To address these challenges, we employ convex autoencoders to map the high-dimensional space into the latent space in a provably correct manner and develop a novel regression technique that enables sound reasoning about inclusion dynamics.

The contributions of this work are four-fold: (i) a provably correct projection of high-level specifications into a latent space, enabling efficient reasoning over the compressed representation, (ii) a novel formulation of Gaussian Process Regression for inclusion-valued (set-valued) dynamics, which we call *Inclusion GPs*, enabling learning of latent dynamics governed by difference inclusions, (iii) a framework for generating sound finite abstractions in the latent space, based on Inclusion GPs, along with procedures for verifying LTL specifications and mapping satisfaction guarantees back to the original high-dimensional system with proof of correctness, (iv) demonstration of the efficacy of our approach on multiple systems, including a 26-dimensional system controlled by a neural network.

1.1 Related Works

Latent space control: Many works explore the use of a latent space for planning and control. A common focus is on enabling control for high-dimensional systems such as humanoid robotics or systems that derive control from visual observations. Common techniques for control in the latent space include model predictive control [33, 16], reinforcement learning [12], and Hamilton-Jacobi reachability [18]. While these techniques often have great empirical success, they typically lack guarantees on the correctness of the approach which can result in false positives.

Several works have recently appeared to attempt to provide formal guarantees with latent space control, however they often

have strong assumptions on the dynamics or can only demonstrate empirical success. In particular, [18, 31] make use of autoencoders to define a latent space for control, but lack guarantees on their learned latent space dynamics. [10, 3] propose methods to soundly reason about dynamics in a low-dimensional space, but cannot compose their low-dimensional model with LTL specifications and have strong assumptions on the form of the dynamics. [15] develops a theory to correctly reason about dynamics in a latent space, but has no method to soundly define the latent domain, preventing the construction of a sound abstraction. We should also stress that various works make use of PCA to identify a low dimensional representation a system for control [17, 11], but as noted in [21, 8] without significant structural constraints on the high dimensional representation (e.g. linear dynamics) the latent space identified by PCA is unlikely to preserve the dynamics exactly.

Exceedingly few works attempt to bridge latent space control with formal specifications. [13] demonstrates empirical success in driving a system to satisfy an LTL specification though training a latent space controller, but cannot provide correctness guarantees on the mapping to the latent space nor provide guarantees on satisfying the specification post training. [25] can construct abstractions in a low dimensional space to verify LTL specifications, but require the original dynamics to be known and decomposable.

2 Problem Formulation

Consider a discrete-time dynamical system:

$$\mathbf{x}(k+1) = f(\mathbf{x}(k)) \quad (1)$$

where $\mathbf{x}(k) \in \mathbb{R}^{n_x}$ is a fully-observable, possibly *high-dimensional* state, and $f : \mathbb{R}^{n_x} \rightarrow \mathbb{R}^{n_x}$ is a Lipschitz continuous, possibly *unknown* function. Intuitively, System (1) represents an autonomous system operating under a closed-loop controller that may be partially or entirely unknown due to AI (black-box) components. An example is a robot navigating a room using a neural network controller that relies on LiDAR measurements and a desired goal orientation. In this case, \mathbf{x} consists of both the robot's state variables and the LiDAR readings, making n_x potentially very large.

An infinite *trajectory* of System (1) is written as $\omega_{\mathbf{x}} = \mathbf{x}(0)\mathbf{x}(1)\dots$ and the set of all infinite trajectories is denoted as $\Omega_{\mathbf{x}}$. We are interested in the temporal properties of System (1) trajectories in a subset $X \subset \mathbb{R}^{n_x}$ w.r.t. a set of regions $R = \{r_1, \dots, r_l\}$, where $r_i \subseteq X$. In this work, we assume sets r_1, \dots, r_l , and X are convex.

To specify and reason about temporal properties, we first define a set of atomic proposition $\Pi = \{p_1, \dots, p_l\}$, where p_i is true iff $\mathbf{x} \in r_i$. Let $L : X \rightarrow 2^{\Pi}$ be a labeling function that assigns to each state the set of atomic propositions that are true at that state. Then, the *observation trace* of trajectory $\omega_{\mathbf{x}}$ is $\rho = \rho_0 \rho_1 \dots$ where $\rho_k = L(\omega_{\mathbf{x}}(k))$ for all $k \geq 0$. To express the desired temporal properties, we use Linear Temporal Logic (LTL) [4].

DEFINITION 1 (LTL). *Given a set of atomic propositions Π , an LTL formula is defined recursively as*

$$\varphi = p \mid \neg \varphi \mid \varphi \vee \varphi \mid \bigcirc \varphi \mid \varphi \mathcal{U} \varphi$$

where $p \in \Pi$, \neg ("not") and \vee ("or") are Boolean operators, and \bigcirc ("next") and \mathcal{U} ("until") are temporal operators.

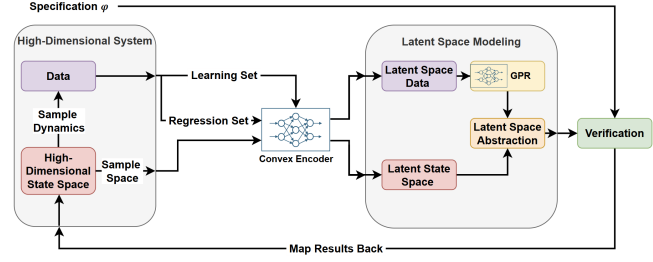


Figure 1: A flowchart of the method used in this paper. From the high-dimensional state space, we gather data. This data is used to train an encoder (Learning Set). We then map the data (Regression Set) and the environment through the encoder, deep kernel GPR is used to learn the latent dynamics from the latent data and the GPR model is composed with the latent environment to create an abstraction. Verification is performed on the abstraction with respect to the specification and results are mapped back to the original environment.

The operators \wedge ("and"), \square ("always"), and \diamond ("eventually") can be defined using \neg , \vee , and \mathcal{U} .

The semantics of LTL are defined over infinite traces [4] and provided in Appendix A.1. We say infinite trajectory $\omega_{\mathbf{x}}$ satisfies formula φ , denoted by $\omega_{\mathbf{x}} \models \varphi$, if its observation trace satisfies φ .

Given an LTL formula φ , our goal is to identify a set of initial states, from which trajectories of System (1) satisfy φ . However, since System (1) is possibly high-dimensional and unknown, we assume the availability of an i.i.d. dataset $D = \{(x_i, x_i^+)\}_{i=1}^m$, where $x_i^+ = f(x_i)$. Our problem can then be stated as follows.

PROBLEM 1 (VERIFICATION). *Consider System (1) in a convex set X with the set of convex regions of interest R , and the associated set of atomic proposition Π . Given dataset $D = \{(x_i, x_i^+)\}_{i=1}^m$ of i.i.d. samples of System (1) and LTL formula φ over Π , find a maximal initial set $X_0 \subseteq X$ such that for every $x_0 \in X_0$ the system is guaranteed to satisfy φ , i.e., $\omega_{\mathbf{x}} \models \varphi$ for every $\omega_{\mathbf{x}}(0) \in X_0$.*

While Problem 1 may resemble a classical verification problem, the fact that f is both high-dimensional and unknown makes verification highly challenging. To address this challenge, a key element of our approach is to map the high-dimensional system to a lower-dimensional representation using an autoencoder. This reduction, however, must be performed carefully to ensure that the latent (low-dimensional) representation remains a sound abstraction of the original system, thereby preserving the desired formal guarantees. We guarantee a sound abstraction by restricting the class of functions that the autoencoder can represent and reasoning with inclusion dynamics in the latent space, as the mapping in is general not one-to-one.

To identify the set of initial states that satisfy the specification, we adopt a finite-abstraction-based approach. An overview of the approach is shown in Fig. 1. Our method begins by learning an autoencoder that maps the system to a lower-dimensional latent space (Section 4.2). In this latent space, we construct a Nondeterministic Transition System (NTS) abstraction (Section 4.3) using (deep kernel) Gaussian Process Regression (GPR) to accurately model the system dynamics (Section 4.4). From the resulting NTS, existing

verification techniques can then be applied to determine which states satisfy the given specification. Finally, we map the verification results obtained in the latent space back to the original state space (Section 5.1).

3 Background

Here, we provide an overview of GP Regression (GPR) and the learning error bounds used in our method, and we introduce the key notation employed throughout our framework.

3.1 Gaussian Process Regression

Let \mathcal{D} be a given dataset $\mathcal{D} = \{(x_i, y_i)\}_{i=1}^m$ obtained from sampling a function of the form $y = \Psi(x) + v$, with $x \in \mathbb{R}^d$ and $y \in \mathbb{R}$. GPR provides a method to predict the output of Ψ at a new point x^* using the dataset \mathcal{D} . A GP is a collection of random variables, such that any finite collection of those random variables is jointly Gaussian [22]. GPR starts by placing a Gaussian prior over Ψ through use of a kernel $\kappa : \mathbb{R}^d \times \mathbb{R}^d \rightarrow \mathbb{R}_{\geq 0}$. Then, under the assumption that v is a zero-mean Gaussian independent random variable with variance σ_n^2 for any new input x^* , a GP produces a posterior prediction of Ψ conditioned on \mathcal{D} with a mean $\mu_{\mathcal{D}}(x^*)$ and variance $\sigma_{\mathcal{D}}^2(x^*)$ as:

$$\mu_{\mathcal{D}}(x^*) = K_{x^*, X}(K_{X, X} + \sigma_n^2 I)^{-1} Y, \quad (2)$$

$$\sigma_{\mathcal{D}}^2(x^*) = K_{x^*, x^*} - K_{x^*, X}(K_{X, X} + \sigma_n^2 I)^{-1} K_{X, x^*}, \quad (3)$$

where $X = [x_1, \dots, x_m]^T$ and $Y = [y_1, \dots, y_m]^T$ are respectively the vectors of input and output data, $K_{X, X}$ is a matrix whose i -th row and j -th column is $\kappa(x_i, x_j)$, and $K_{X, x^*} = K_{X, X}^T$ are vectors whose i -th entry is $\kappa(x_i, x^*)$. Deep Kernel Learning (DKL) is an extension of GP regression which incorporates a Neural Network ψ into a base kernel as $\kappa(\psi(x), \psi(x'))$. DKL that has been shown to enable more accurate mean predictions, smaller posterior variance predictions, and faster abstraction generation [24].

3.1.1 GP Error Bounds. Under the assumption that Ψ is Lipschitz and lives in the Reproducing Kernel Hilbert Space (RKHS) of kernel κ , then there exists some constant $B > 0$ such that $\|\Psi(\cdot)\|_{\kappa} \leq B$ in the compact domain X . For many kernels κ used in practice, such as the squared exponential kernel, the RKHS is dense in the space of continuous functions [28].

Under this assumption, GPR can be extended to the setting where v has bounded support with error bounds as follows

PROPOSITION 1 ([23], THEOREM 2). *Let Ψ live in the RKHS of κ with norm $B > 0$, and let $G = (K_{X, X} + \sigma_n^2 I)^{-1}$, $d^* \leq \Psi(X)^T G \Psi(X)$. If noise v is zero-mean and has a finite support σ_v , then it holds that, for every $x \in X$ and with $\sigma_n > 0$,*

$$|\mu_{\mathcal{D}}(x) - \Psi(x)| \leq \sigma_{\mathcal{D}}(x) \sqrt{B^2 - d^*} + \Lambda_x \quad (4)$$

where $\Lambda_x = \sum_{i=1}^m \sigma_v |[K_{X, X} G]_i|$.

This can be further extended to the noise-free scenario, resulting in the bound $|\mu_{\mathcal{D}}(x) - \Psi(x)| \leq \sigma_{\mathcal{D}}(x) \sqrt{B^2 - d^*}$.

3.2 Notation

Given a high n_x -dimensional state x , an *encoder* $h_{enc} : \mathbb{R}^{n_x} \rightarrow \mathbb{R}^{n_p}$ maps x to an n_p -dimensional state $z = h_{enc}(x)$. We refer to \mathbb{R}^{n_p} as the *latent space*. A *decoder* $h_{dec} : \mathbb{R}^{n_p} \rightarrow \mathbb{R}^{n_x}$ then maps a $z \in \mathbb{R}^{n_p}$

to a state x . Given a set of points A , $\text{Conv}(A)$ defines the convex hull of the set. In a metric space \mathbb{R}^{n_x} , $\mathcal{B}_r(x) = \{x' \in \mathbb{R}^{n_x} \mid \|x - x'\| \leq r\}$ denotes a ball of radius $r \geq 0$ centered at $x \in \mathbb{R}^{n_x}$.

We use the following notation to describe set relations from the original and latent space. Let X_z be the set of all $x \in \mathbb{R}^{n_x}$ that map to the same $z \in \mathbb{R}^{n_p}$, i.e., $X_z := \{x \mid h_{enc}(x) = z\} =: \text{Pre}_{h_{enc}}(z)$. X_z is called the *pre-image* of z through h_{enc} . Also, we use X'_z to denote the posterior of the set X_z under the dynamics of System (1), $X'_z := \{f(x) \mid x \in X_z\} =: \text{Post}_f(X_z)$. Encoding the set X'_z produces the set $\mathcal{Z}' = \{h_{enc}(x') \mid x' \in X'_z\} = \text{Post}_{h_{enc}}(X'_z)$.

4 Finite Abstraction in the Latent Space

In this section, we present our method of constructing a sound finite-abstraction in the latent space. It involves training an autoencoder coupled with deep kernel learning, i.e., GPR, in the latent space.

We first observe that when the latent space has a lower dimension than the original space, i.e., $n_p < n_x$, the resulting latent dynamics may be neither injective nor deterministic. In particular, when the dimensionality of System (1) is reduced beyond its minimal realization, i.e., the smallest number of parameters required to exactly reconstruct the observations, the evolution in the latent space is governed by a *inclusion dynamics* as defined below.

DEFINITION 2 (LATENT INCLUSION DYNAMICS). Consider System (1) and encoder $h_{enc} : \mathbb{R}^{n_x} \rightarrow \mathbb{R}^{n_p}$. For a latent point $z \in \mathbb{R}^{n_p}$, let $X_z = \text{Pre}_{h_{enc}}(z)$ be its pre-image and $X'_z = \text{Post}_f(X_z)$ be the posterior of X_z under the dynamics of System (1). Then, latent space inclusion dynamics of System (1) are defined as

$$z(k+1) \in g(z(k)), \quad (5)$$

where $g : \mathbb{R}^{n_p} \rightarrow 2^{\mathbb{R}^{n_p}}$ is given by $g(z(k)) = \text{Post}_{h_{enc}}(X'_{z(k)})$.

If the latent space is a correct minimal realization, then $g(z(k))$ is a singleton. This is illustrated in the following example.

Example 1. Consider the system

$$\begin{bmatrix} x^+ \\ y^+ \end{bmatrix} = \begin{bmatrix} 1 & 1 \\ 0.1 & -1 \end{bmatrix} \begin{bmatrix} x \\ y \end{bmatrix}$$

and an encoder that induces a non-invertible change in variable, e.g., $h_{enc}(\begin{bmatrix} x \\ y \end{bmatrix}) = x + y$ where the latent state $z = x + y$. To compute the evolution of the latent dynamics, we can write

$$z^+ = x^+ + y^+ = (x + y) + (0.1x - y) = 1.1x.$$

Hence, the evolution of z is uniquely determined by x , but in the latent space, we do not have access to x . Therefore, z^+ is not a single-valued function of z ; it is set valued:

$$z^+ \in \{1.1x \mid x \in \mathbb{R}, \exists y \text{ s.t. } x + y = z\}$$

Hence, in a latent space of lower dimension than the minimal realization, the system evolves according to inclusion dynamics. In a correct minimal realization, the dynamics evolve according to a difference equation. By denoting the evolution in the latent space with the singleton $\{f(x)\}$, the system can still be described with inclusion dynamics.

Our second observation is that, generating a sound abstraction requires preserving the regions of interest in R in the latent space. We refer to this property as the *interpretability* of the latent space.

As both the state and labels are observations of the original system, reducing dimensionality in an uninformed manner can cause significant difficulty in verifying the systems properties.

These two observations highlight the need for an encoder h_{enc} that produces an interpretable latent space and supports accurate learning of inclusion dynamics. To achieve this, we impose structural constraints on h_{enc} and inform its training with the knowledge that latent evolution follows inclusion dynamics. We describe the structural constraints below.

4.1 Encoder Architecture

Our framework is designed around generating an interpretable latent space where the inclusion dynamics behave well. To this end, we first restrict the encoder to a class of networks that are convex functions, enabling efficient and provably correct reasoning about latent regions of interest (see Section 4.3.1 for details). Convexity is enforced by constraining all weights after the first hidden layer to be nonnegative and by using activation functions that are both convex and monotonic. Networks of this form are known as *Input Convex Neural Networks* (ICNNs) [1]. Although constraining weights may appear to limit representational power, prior work has shown that ICNNs can be made highly expressive through the use of skip connections. ICNNs are typically employed to enable tractable optimization and inference [26]; to the best of our knowledge, their use as an autoencoder has not been explored. Our approach makes use of convexity to map regions to \mathbb{R}^{n_p} efficiently.

To further regulate the behavior of inclusion dynamics in the latent space, we impose additional structural requirements on the ICNN. Specifically, we restrict activation functions to be strictly monotonic (e.g., SoftPlus), require the first layer and all skip layers to be injective (i.e., each skip layer must have output dimension at least n_x , which is a nonrestrictive condition that also enhances expressivity), and enforce full-rank weight matrices in every layer. We refer to this architecture as a *Connected Input-Connected Output* (CICO) network. These architectural constraints guarantee that the evolution set $g(z(k))$ of the inclusion dynamics in (5) remains connected when f is continuous.

LEMMA 1 (CONNECTED INCLUSION DYNAMICS). *Consider System (1), neural network encoder $h_{enc} : \mathbb{R}^{n_x} \rightarrow \mathbb{R}^{n_p}$, and the corresponding latent inclusion dynamics (5). Furthermore, for the latent point $z \in \mathbb{R}^{n_p}$, let $X_z = \text{Pre}_{h_{enc}}(z)$ be its pre-image in the original space. If h_{enc} is CICO, then both X_z and $g(z)$ are connected sets.*

The proof is in Appendix A.2. The proof for the connectivity of X_z relies on the fact that full rank affine transformations and strictly monotonic activations each have connected pre-images. Then by continuity of both f and h_{enc} , $\mathcal{Z}' = g(z)$ must be connected.

Based on Lemma 1, the CICO property of h_{enc} ensures that latent inclusion dynamics g in (5) always outputs a connected set, enabling us to learn g in a provably correct and non-conservative manner using Gaussian Process Regression (see Section 4.4 for details).

We note that if the activation functions of h_{enc} are not strictly monotone, then the pre-image $\text{Pre}_{h_{enc}}(Z)$ of a connected set $Z \subset \mathbb{R}^{n_p}$ can easily be disconnected, i.e., the encoder induces folding. Consider the ReLU activation; since the activations act dimension wise on the outputs of the affine transformation, ReLU can easily map disjoint regions of the input to the same value after multiple

layers (e.g., two disjoint sets fall into the negative range of the pre-activation after a layer and then ReLU maps them both to 0). In contrast, strictly monotonic activation functions are injective and homeomorphic on their domains, which prevents folding.

4.2 Learning a Latent Space

While autoencoders and latent dynamic models are a common approach to dimensionality reduction and control, our novelty comes from the representation of the dynamics as inclusion dynamics and the constraints we impose on the architecture of the encoder to enable a correct representation of high-dimensional sets in the latent space. To learn the interpretable latent space, we define three separate neural networks: (i) the encoder h_{enc} , (ii) a latent space dynamics network \hat{g} , and (iii) the decoder h_{dec} . The latent space dynamics network \hat{g} is defined as a set-valued neural network to model inclusion dynamics during the training. That is, \hat{g} takes in a point z and outputs a ball of radius $\hat{g}_r(z)$ centered at $\hat{g}_c(z)$, i.e., $\hat{g}(z) = \mathcal{B}_{\hat{g}_r(z)}(\hat{g}_c(z))$.

When training the networks, we propose the following loss function that consists of several objective functions to identify a latent space where an informative abstraction can be constructed, while training all the networks simultaneously, i.e.,

$$h_{enc}, \hat{g}, h_{dec} = \arg \min_D L(x, x')$$

where

$$L(x, x') = \sum_{j=1}^4 \alpha_j L_j(\{x, x'\}) + \alpha_5 L_5(x, x'), \quad (6a)$$

$$L_1(x) = \max \{0, \|h_{enc}(f(x)) - \hat{g}_c(h_{enc}(x))\| - \hat{g}_r(h_{enc}(x))\}, \quad (6b)$$

$$L_2(x) = \hat{g}_r(h_{enc}(x)), \quad (6c)$$

$$L_3(x) = \|x - h_{dec}(h_{enc}(x))\|, \quad (6d)$$

$$L_4(x) = \mathbb{E}_{q(z|x)} [-\log p(x|z)] + \text{KL}(q(z|x) \| p(z)), \quad (6e)$$

$$L_5(x, x') = \| \|x - x'\|_{A_X} - \|h_{enc}(x) - h_{enc}(x')\|_{A_Z} \|, \quad (6f)$$

and $\alpha_j > 0$ are weights for each objective. L_1 enforces that the evolution of the dynamics when mapped to the latent space should be captured by the ball predicted by \hat{g} . As this is trivially satisfied if the ball is of infinite radius, L_2 is defined to penalize the size of the set. L_3 is a standard autoencoder loss that attempts to learn an architecture where the composition $h_{dec}(h_{enc}(\cdot))$ is an Identity function. Loss functions $L_1 - L_3$ encourage a latent space where dynamics do not grow rapidly, which helps construct an abstraction with sparse transitions, and requires the latent space to remain informative enough to decode accurately.

Objectives L_4 and L_5 are introduced to further encourage the expressivity of the latent space. L_4 is a required loss term when using a Variational Autoencoder and acts as a regularization term during training that prevents the collapse of the latent space; post training the encoder must be used as a deterministic function. L_5 is a term that encourages the notion of distance to be similar between the original space and the latent space, with weighting matrices A_X, A_Z ; similarly to L_4 this helps prevent the collapse of the latent space and encourages regions to be separated in the latent domain.

It should be noted, that while \hat{g} and h_{dec} are required for the encoder h_{enc} to be well informed during training, they hold no

guarantees on correctness and cannot be directly used to create the abstraction. We also note that h_{dec} can be defined as a set-valued neural network, to more accurately represent how points in the latent space are mapped to sets in the high-dimensional space.

4.3 Nondeterministic Transition System Abstraction

In the latent space, we construct an NTS abstraction.

DEFINITION 3 (NTS). A Transition System (TS) is a tuple $\mathcal{N} = (Q, T, L, AP)$, where Q is a finite set of states, $T : Q \times Q \rightarrow \{0, 1\}$ is a transition function such that $T(q, q') = 1$ if q' is a successor state of state $q \in Q$, AP is a set of atomic propositions, and $L : Q \rightarrow 2^{AP}$ is a labeling function that assigns to each $q \in Q$ a subset of AP . \mathcal{N} is called Non-deterministic (NTS) if $\sum_{q' \in Q} T(q, q') > 1$.

An infinite path on NTS \mathcal{N} starting at q_0 is defined as $\omega_{q_0} = q_0 q_1 q_2 \dots$ where $T(q_i, q_{i+1}) = 1$ and the set of all infinite paths from q is denoted as Ω_q . Note that from an initial state q there may exist multiple paths due to non-determinism in T . We say $\omega_q \models \varphi$ if its observation trace $\rho = \rho_0 \rho_1 \dots$ where $\rho_k = L(\omega_q(k))$ satisfies φ . Then $\Omega_q \models \varphi$ iff $\omega_q \models \varphi$ for all $\omega_q \in \Omega_q$.

To construct a finite NTS of System (1) in the latent space, we must first define the latent domain and its partitioning to obtain the set of discrete states Q . Next, we need a method to label regions of interest in the latent space that correspond to the regions of R to define L and AP , and a method to identify transitions between discrete states to construct T . We begin by discussing how regions in \mathbb{R}^{n_x} are mapped into the latent space.

4.3.1 Mapping Regions of Interest. To reason about the temporal properties of the system in the latent space, it is necessary to map the regions of interest $r \in R$ from \mathbb{R}^{n_x} to \mathbb{R}^{n_p} . To retain guarantees on the correctness of the abstraction, it is necessary to have guaranteed under- and over-approximations of these regions in the latent space. Translating regions down to the latent space can be a challenge when using a generic encoder architecture, and is akin to the neural network verification problem where given an input set we would like to under- or over-approximate the output set of the network, e.g., [32]. These methods are generally known to work best when given small input sets. Hence to get tight approximations, these methods require partitioning the high-dimensional domain, which could be computationally expensive due to the exponential growth of the size of a partition with the dimensionality. Arbitrary encoder architectures can also induce folding in the domain, resulting in disjoint regions mapping to the same area in the latent space which can make correct labeling a challenge, hence our restriction of the architecture to CICO networks (see Section 4.1).

With h_{enc} as a CICO network, we guarantee that a convex input set is always mapped to a convex output set. This notion allows us to use efficient sampling based methods to map a high-dimensional convex region down with a guaranteed under-approximation of the region in the latent space, while avoiding the computational complexity of standard neural network verification methods. In particular, by sampling points from a convex set, we can map the points to the latent space and define a convex hull from these points. This hull is a guaranteed under-approximation of the mapped region.

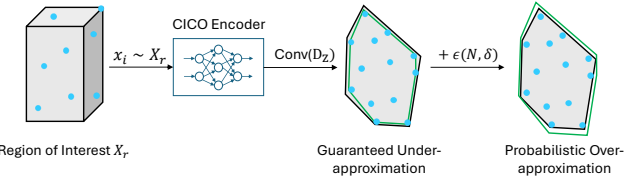


Figure 2: Visualization of embedding a region X_r into the latent space, with the true boundary of the set shown in black, sampled points x_i in cyan, and the Convex Hull under/over-approximations shown in green.

Given convex set $r_i \subset \mathbb{R}^{n_x}$, the encoding of this set $r_{Z,i} = \text{Post}_{h_{enc}}(r_i)$ is also convex. Directly calculating $r_{Z,i}$ is generally infeasible; however, we can sample a set of N points from r_i and map each point through h_{enc} to define a set in \mathbb{R}^{n_p} where the convex hull is a subset of $r_{Z,i}$.

We can also over-approximate $r_{Z,i}$ with high confidence through sampling by adapting the method proposed in [14], called ϵ -RandUp.

PROPOSITION 2 (ϵ -RANDUP [14], THEOREM 2). Let $D_Z = \{h_{enc}(x) \mid x \sim r \in R\}_{i=1}^N$ be a set of encoded points sampled from region r and $r_Z = \text{Post}_{h_{enc}}(r)$ be the true image of r through h_{enc} . Also, let L_h be the Lipschitz constant of h_{enc} . Then, there exists an $\epsilon(N, \delta) \geq 0$ such that with probability at least $1 - \delta$,

$$r_Z \subset \text{Conv}(D_Z) \oplus \mathcal{B}_{\epsilon(N, \delta)}(0), \quad (7)$$

where \oplus denotes a Minkowsky sum, $\epsilon(N, \delta)$ satisfies $\delta = D(\partial r, \frac{\epsilon}{2L_h})(1 - \Lambda_{L_h}^\epsilon)^N$, $D(\partial r, \frac{\epsilon}{2L_h})$ is a covering number for boundary ∂r , and $\Lambda_{L_h}^\epsilon$ is a lower bound on sampling points within an $\frac{\epsilon}{2L_h}$ ball of each other.

We can formally bound $\epsilon(N, \delta)$ with $L_h \left(\frac{v_{n_x}}{Nv_{n_p}} \log \frac{(4L_h \sqrt{n_x})^{n_x}}{\delta} \right)^{1/n_p}$ where v_i is the volume of an i -dimensional ball, as under the assumption that r is defined as a subset of a unit ball and is uniformly sampled we can take $D(\partial r, \epsilon/2L_h) \leq (4L_h \sqrt{n_x})^{n_x}$ and $\Lambda_{L_h}^\epsilon > \frac{v_{n_p}}{v_{n_x} L_h^{n_p}} \epsilon^{n_p}$ [14]. Note that ϵ -RandUp does not require h_{enc} to be a convex function or $r \in R$ to be a convex set, but the convexity of h_{enc} enables us to identify both under- and over-approximations that are arbitrarily tight by increasing the number N of samples used ([14], Theorem 1). A visualization of the process is shown in Figure 2.

We highlight that, through this sampling-based method, the under-approximation of r_Z is guaranteed deterministically, whereas the over-approximation holds with high confidence. Alternate methods, e.g., [32], can be used for a deterministic over-approximation, though at the cost of reduced efficiency.

4.3.2 States and Labels. To define NTS states and labels, we first map X into the latent space, i.e., $\text{Post}_{h_{enc}}(X)$, and compute its under-approximation. Using the sampling-based method described above, we obtain $Z = \text{Conv}(\{h_{enc}(x_i) \mid x_i \sim X\}_{i=1}^N) \subseteq \text{Post}_{h_{enc}}(X)$; we refer to Z as the *latent domain*. We then partition Z into a set of regions $\bar{Q} = \{q_0, \dots, q_{|\bar{Q}|}\}$, e.g., via a non-uniform grid. With an abuse of notation, we use q to refer to both the discrete state $q \in Q$ of the NTS and the region $q \subseteq Z$ that it occupies. We define the set of states for the NTS $Q = \bar{Q} \cup \{q_u\}$, where $q_u = \mathbb{R}^p \setminus \bigcup_{q \in \bar{Q}} q$ is the set of points lying outside the partition of the latent domain Z .

To ensure that the labeling for each region $r_i \in R$ is done correctly in the latent space, we follow the method outlined in [9] and begin by representing r_i and its complement $r_{n,i} = X \setminus r_i$ with new atomic propositions $p_i, p_{n,i}$, where $p_{n,i}$ then represents $\neg p_i$. The atomic propositions for the NTS are then defined as

$$AP := \Pi \cup \{p_{n,1}, \dots, p_{n,l}\}. \quad (8)$$

To enable mapping of the regions with correct under- and over-approximations for the purpose of labeling, we first partition $r_{n,i}$ into a set of convex regions $r_{n,i}^k$ such that $r_{n,i} = \cup_k r_{n,i}^k$. Then, we construct labeling regions that correspond to r_i in the latent space according to

$$\check{r}_{Z,i} = c_{Z,i} \setminus \cup_k r_{n,i}^k \quad (9a)$$

$$\hat{r}_{Z,i} = c_{Z,i} \oplus \mathcal{B}_{\epsilon(N,\delta)}(0), \quad (9b)$$

where

$$c_{Z,i} = \text{Conv}(\{h_{enc}(x) | x \sim r_i\}_{i=1}^N), \quad (9c)$$

$$r_{Z,n,i}^k = \text{Conv}(\{h_{enc}(x) | x \sim r_{n,i}^k\}_{i=1}^N) \oplus \mathcal{B}_{\epsilon(N,\delta)}(0). \quad (9d)$$

Note that the under-approximation $\check{r}_{Z,i}$ is defined using an over-approximation of $X \setminus r_i$. We use $\hat{r}_{Z,i}$ to define the set of states with label p_i . This is necessary to ensure that no state in $X \setminus r_i$ receives the label p_i when mapped to the latent space. Intuitively, $c_{Z,i}$ is an under-approximation of where r_i can map to, but not an under-approximation of where r_i exclusively maps to.

This construction guarantees we under-approximate both the region r_i and its negation in the latent space, as well as the set of states in the NTS that are associated with that region. We define the NTS labeling function $L : Q \rightarrow 2^{AP}$ such that $p \in L(q)$ if $q \subset \check{r}_{Z,i}$, and $p_{n,i} \in L(q)$ if $q \subset Z \setminus \hat{r}_{Z,i}$.

LEMMA 2 (CONSERVATIVE LABELING). *For a point $x \in X$, let $q_x \ni h_{enc}(x)$ denote the latent region in the partition Q that contains $h_{enc}(x)$, and with an abuse of notation, let $L : X \rightarrow 2^{AP}$ or $L : Q \rightarrow 2^{AP}$, where AP is defined in Eq. (8). Under the construction of the latent space described in Section 4.3.1 and labeling procedure described in Section 4.3.2, with high-confidence, it holds that $L(q_x) \subseteq L(x)$.*

Hence we capture (conservatively) all of the regions R (and their negations) by the labels in N , a detailed proof is available in Appendix A.3. We first translate φ to NNF as $\text{NNF}(\varphi)$ (see Appendix A.1 for details), and then replace every $\neg p_i$ in $\text{NNF}(\varphi)$ with $p_{n,i}$. Then any trace that satisfies $\bar{\varphi}$ over AP will also satisfy φ over Π [9].

REMARK 1. *As points outside of original domain X could map into latent domain Z , some minor bookkeeping is required for any x in dataset D that is not in X . Once Z is defined, we can trivially enforce that $h_{enc}(x) \notin Z$ if $x \notin X$, by mapping points outside of X to points outside of Z . This can be achieved in a non-convex manner as it does not impact the correctness of the mapping of regions.*

REMARK 2. *For reach-avoid specifications, labeling can be simplified by using Eq. (9b) to identify over-approximations of the regions to avoid in the latent space and Eq. (9a) to under-approximate regions that must be reached, without needing additional propositions for their negations.*

4.4 NTS Transitions: Modeling the Latent Inclusion Dynamics

We propose a novel approach to model inclusion dynamics accurately based on GPR. From an GP model, we then build off of existing methods, e.g., [27, 24], to generate a NTS abstraction transitions.

4.4.1 Inclusion GP. By Lemma 1, the latent space inclusion dynamics g in Eq. (5) outputs connected sets, i.e., $g(z) = Z'$ is a connected set. We can then consider a family of continuous functions $g_c : \mathbb{R}^{np} \rightarrow \mathbb{R}^{np}$ such that $g := \{g_c | c \in [a, b] \subset \mathbb{R}\}$. We formalize this notion in the following Lemma.

LEMMA 3. *Let $g : \mathbb{R}^{np} \rightarrow 2^{\mathbb{R}^{np}}$ be latent space dynamics induced by CICO h_{enc} and f . Then there exists an infinite set of continuous functions parameterized by c such that $g := \{g_c | c \in [a, b] \subset \mathbb{R}\}$ and $g_c : \mathbb{R}^{np} \rightarrow \mathbb{R}^{np}$.*

The proof relies on CICO h_{enc} and continuous f , resulting in $g(z)$ being Hausdorff continuous. A detailed proof is provided in Appendix A.4.

Since for each choice of $c \in [a, b]$, g_c is a continuous function and each realization of $g(z)$ returns a single element, GPR can be used to learn the j -th component of g_c . However, in our setting we do not have data as $([z_i, c_i], z_i^+)$, but instead have data as (z_i, z_i^+) . To enable GPR, we must learn the unobserved variable c_i that matches the data (z_i, z_i^+) . We draw inspiration from Gaussian Process Latent Variable Models (GPLVM) [30], which are employed to identify an input data set for GPR when only given an observation dataset. GPLVMs have commonly been used for generative modeling and dimensionality reduction methods, but unlike our approach GPLVMs do not typically have an interpretable latent space which makes predicting the evolution of dynamics infeasible.

Following a GPLVM approach, we first regress over the encoded data $\{(z_i, z_i^+)\} = \{(h_{enc}(x_i), h_{enc}(x_i^+))\}$ and learn a $c_i \in [a, b]$ for each (z_i, z_i^+) resulting in an augmented dataset $\{([z_i, c_i], z_i^+)\}$. The resulting GP kernel is then $\kappa : \mathbb{R}^{np+1} \times \mathbb{R}^{np+1} \rightarrow \mathbb{R}_{\geq 0}$. Using methods outlined in [24], we learn a deep kernel model from the augmented data set where the j -th component of g_c is modeled with $\mu_D^{(j)}(z, c)$.

When predicting with this model, we capture the inclusion dynamics g by predicting over the full range of c at a point as $(z^*, [a, b])$. We refer to this GP model as an *Inclusion GP*. A visualization of the Inclusion GP prediction is shown in Figure 3. Notice how the predicted output set from a single point spans the range of observed evolutions and accurately captures non-determinism.

Intuitively, an Inclusion GP captures the evolution of a non-deterministic system by predicting with an infinite set of functions. This formulation allows us to use RKHS reasoning with GP error bounds for each individual g_c . As individual g_c are not well defined, we extend this reasoning over inclusion dynamics as follows.

THEOREM 2 (TRANSITION FUNCTION CONSTRUCTION). *Let g be as in Lemma 3, and constants $B_j > 0$ and $d_j^* \geq 0$ hold for each $g_c^{(j)}$ according to Proposition 1, and $\epsilon^{(j)}(z, c) = \sigma_D(z, c) \sqrt{B_j^2 - d_j^*}$, then*

$$g^{(j)}(z) \subseteq [\check{\mu}_D^{(j)}(z) - \bar{\epsilon}^{(j)}(z), \hat{\mu}_D^{(j)}(z) + \bar{\epsilon}^{(j)}(z)], \quad (10)$$

where $\bar{\epsilon}^{(j)}(z) = \max_c \epsilon^{(j)}(z, c)$, and $\check{\mu}_D^{(j)}(z), \hat{\mu}_D^{(j)}(z)$ are the min and max of $\mu_D^{(j)}(z, c)$ over c respectively.

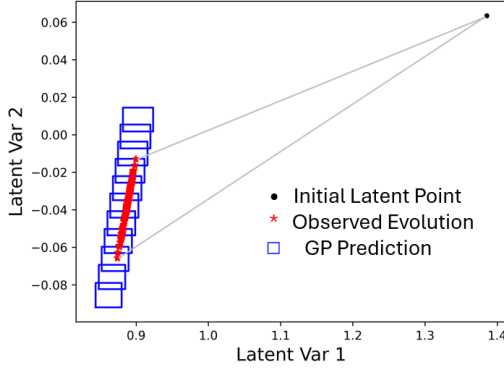


Figure 3: Visualization of Inclusion GP predictions. The initial latent variables z^* is shown as a black dot (top-right), observed evolutions z_i^+ as red stars (multiple samples of $h_{enc}(X'_{z^*})$), the predicted evolution for 10 c^* values of the Inclusion GP with blue rectangles $(\mu_D^{(j)}(z^*, c^*) \pm \sigma_D^{(j)}(z^*, c^*)\sqrt{B^2 - d^*})$.

PROOF. The proof is straight-forward. By definition $\epsilon^{(j)}(z, c) \leq \bar{\epsilon}^{(j)}(z)$, then according to Proposition 1 for all c

$$|\mu_D^{(j)}(z, c) - g_c^{(j)}(z)| \leq \bar{\epsilon}^{(j)}(z), \quad (11)$$

Let $\text{Im}^{(j)}(z) = \{w \mid w = g_c^{(j)}(z) \forall c \in [a, b]\}$. Then it follows that $|\mu_D^{(j)}(z) - \min \text{Im}^{(j)}(z)| \leq \bar{\epsilon}^{(j)}(z)$ and similarly with the maximum. Then under the assumption that $g := \{g_c \mid c \in [a, b]\}$, g is contained in the union of all error sets and the theorem is complete. \square

4.4.2 NTS Transition Function. Using an Inclusion GP, region $q \subset \mathbb{R}^{np}$ is propagated for a subset $u \subset [a, b]$ as

$$\text{Im}(q, u) = \{w \mid w^{(j)} = \mu_D^{(j)}(z, c), c \in u, z \in q\}. \quad (12)$$

For a region q and subset u , let $\epsilon_{q,u}^{(j)} = \sup_{z \in q, c \in u} \epsilon^{(j)}(z, c)$, and let the worst case regression error over a region q be $\epsilon^{(j)}(q, u) = \sup_{z \in q, c \in u} |\mu_D^{(j)}(z, c) - g_c^{(j)}(z)|$. Then, $\epsilon^{(j)}(q, u) \leq \epsilon_{q,u}^{(j)}$. The transition from $z \in q$ to q' under dynamics g can be over-approximated according to the following proposition, a modified form of [27, Theorem 1] that accounts for the noise-free regression setting.

PROPOSITION 3 ([27], THEOREM 1). Let $\bar{\epsilon}^{(j)}(\epsilon)$ be a region that is obtained by expanding each dimension of q' with the corresponding scalars in $\epsilon_{q,u}$. Also let U be a partition of $[a, b]$ such that $\bigcup_{u \in U} u = [a, b]$. Define the transition function of the NTS \mathcal{N} abstraction as

$$T(q, q') = \max_{u \in U} \left(\mathbb{1}_{\bar{\epsilon}^{(j)}(\epsilon)}(\text{Im}(q, u)) \right), \quad (13)$$

where $\mathbb{1}_W(H) = 1$ if $W \cap H \neq \emptyset$ and 0 otherwise. Then, it holds that

$$\forall z \in q, \quad g(z) \subseteq \{z' \in q' \mid q' \in Q, T(q, q') = 1\}. \quad (14)$$

We finalize the construction of the abstraction \mathcal{N} by making q_u an absorbing state, i.e., $T(q_u, q') = 1$ if $q' = q_u$ and 0 otherwise. T then conservatively captures the behavior of the inclusion dynamics under discretization, i.e., for $z' \in q'$ and $z \in q$ if $z' \in g(z)$ then $T(q, q') = 1$. With the T defined, the NTS is completed.

DEFINITION 4 (SOUND ABSTRACTION). Let $\mathcal{R} \subseteq \mathbb{R}^{n_x} \times Q$ define a relation such that $(x, q) \in \mathcal{R}$ if $h_{enc}(x) \in q$. NTS \mathcal{N} is a sound abstraction of System (1) in domain X , if for any trajectory ω_{x_0} , $\exists \omega_{q_0} \in \Omega_{q_0}$ s.t. $(\omega_{x_0}(k), \omega_{q_0}(k)) \in \mathcal{R}$ and $L(\omega_{q_0}(k)) \subseteq L(\omega_{x_0}(k))$ for all $k \geq 0$.

THEOREM 3 (SOUND ABSTRACTION). Let NTS \mathcal{N} be constructed with the states and labeling function defined according to Section 4.3, and with a transition function defined according to Proposition 3. Then \mathcal{N} is a sound abstraction for System (1), and for every $(x, q) \in \mathcal{R}$, if all the paths initialized at q in \mathcal{N} satisfy $\bar{\varphi}$, then the trajectory ω_x is guaranteed to satisfy $\bar{\varphi}$, i.e.,

$$\Omega_q \models \bar{\varphi} \implies \omega_x \models \bar{\varphi} \quad \forall (x, q) \in \mathcal{R}. \quad (15)$$

Lemma 2 and Proposition 3 establish \mathcal{N} as a sound abstraction. Then it can be seen that if $\omega_{x_0} \not\models \bar{\varphi}$ there must exist a path ω_{q_0} where $(x_i, q_i) \in \mathcal{R}$ for all $i \geq 0$ s.t. $\omega_{q_0} \not\models \bar{\varphi}$, which implies Eq. (15). A detailed proof of Theorem 3 is available in Appendix A.5.

REMARK 3. We note that while our formulation defines $g(z)$ as a connected set, this is not a requirement to perform Inclusion GPR. If the output is not connected, the same approach can be used, but the GP prediction becomes a conservative connected set representation of the disjoint evolution. Our formulation is designed to have minimal conservatism in the prediction of the latent space dynamics.

4.4.3 RKHS Constants in the Latent Space. As stated in [23], d^* (the parameter used in the GPR error bounded in Proposition 1 and Theorem 2) can be conservatively set to 0 to avoid difficulty in calculating a nontrivial value, as in our case $d^* \leq g_c^{(j)}(Z)^T (K_{(Z,c),(Z,c)} + \sigma_n^2 I)^{-1} g_c^{(j)}(Z)$ would require being able to bound the effect of $g_c(Z)$ on the quadratic form. B can be formally bounded using approaches in [27], and only depends on having a Lipschitz constant for the dynamics. The Lipschitz constant for g can be easily bounded using the constants for h_{enc} and the dynamics in the original space, or bounded using approaches outlined in [34].

5 Verification and Refinement

Given that the NTS is a sound abstraction of System (1) per Theorem 3 in the latent space, we can make use of existing methods for verification against LTL specifications to identify the set of states that are guaranteed to satisfy the specification [4]. Due to the uncertainty introduced by non-determinism and discretization in the latent space, we obtain three sets from verification Q_{yes} (set of states guaranteed to satisfy φ), Q_{no} (set of states that satisfy $\neg\varphi$), and $Q_? = Q \setminus (Q_{yes} \cup Q_{no})$. This uncertainty can result in large volumes of space falling in $Q_?$. To address this, we consider iterative refinement of the abstraction and choose states with the most immediate uncertainty to further discretize, i.e., we choose the states in $Q_?$ that have transitions to either Q_{yes} or Q_{no} to refine. However, we cannot conclude that states x s.t. $h_{enc}(x) \in Q_{no}$ violate φ , but states in Q_{yes} are guaranteed to satisfy φ .

5.1 Decoding

Once the abstraction is verified in the latent space, it is desirable to translate the results back to the high-dimensional system. We approach this by decoding the latent states in a correct manner. Recall that the encoder is a convex function in our formulation. This

enables decoding to be posed as a convex optimization problem, i.e., given a point $z \in Z$ in the latent space we can *exactly* and efficiently decode it through the optimization of $\arg \min_{x \in X} \|h_{enc}(x) - z\|$.

While it may be difficult to find all points x that map to a single z we can relax the problem to instead decode a convex hyperrectangle q from our partition and identify a boundary from the original domain that encodes to this set. The search points for the optimization can be initialized with the decoder as $x_i = h_{dec}(z_i)$ by sampling a set of points in the latent space as $z_i \sim q$. The optimization can then be stopped when any x_i is identified such that $h_{enc}(x_i) \in q$. Let q_c be the center point of q , r_q the vector that defines the radius of the q in each dimension, and denote $(\cdot)^{(j)}$ the j -th dimension of a vector (\cdot) , then this can be formulated with the constrained $(x_i \in X)$ convex optimization

$$\max_j \left(\frac{|h_{enc}(x_i)^{(j)} - q_c^{(j)}|}{r_q^{(j)}} \right) < 1 \quad (16)$$

Then we can use Eq. (16) to identify $\text{Pre}_{h_{enc}}(q) \in X$. The properties of our encoder enforce that the pre-image of a connected set is also connected, hence we can easily over-approximate the pre-image from samples using the same approach described in Section 4.3.1. Alternatively, we can make use of robust pre-image calculation methods for neural networks such as PREMAP [35], which provide a tight under-approximation of the pre-image as a union of polytopes.

6 Case Studies

In this section, we demonstrate the effectiveness of our approach with several case studies, (i) an example that demonstrates that we can reduce dimensionality beyond the minimal realization and still correctly reason about temporal properties, (ii) an example that shows that over-parameterized models can be correctly reasoned about, (iii) an example for a high-dimensional system which traditional abstraction techniques could not reason about without suffering state explosion, and (iv) an example for a high-dimensional system with an LTL specification that can only be satisfied over an infinite horizon.

In each case study, we first learn h_{enc} from a dataset D_{enc} (the Learning Set from Figure 1) and then optimize the unobserved latent variable for the GP model with a separate dataset D_{GP} (the Regression Set from Figure 1). After generating the latent dataset $\{([z_i, c_i], z_i^+)\}_{i=1}^m$, we then learn a deep kernel model that predicts the evolution of the dynamics in the latent space with a network $\psi : \mathbb{R}^{p+1} \rightarrow \mathbb{R}^p$ and optimize the base kernel parameters for each dimension as $\kappa(\psi^{(j)}(z, c), \psi^{(j)}(z', c'))$, following methods outlined in [24]. The first three examples use the LTL specification $\varphi = \neg p_{\text{unsafe}} \mathcal{U} p_{\text{goal}}$, where p_{unsafe} is an atomic proposition that represents unsafe sets including $\mathbb{R}^{n_x} \setminus X$, and p_{goal} is a proposition for the goal. The final example uses a more complex specification of $\varphi = \square(\neg p_{\text{unsafe}}) \wedge \diamond(p_{\text{goalA}}) \wedge \diamond(p_{\text{goalB}})$ where p_{goalA} and p_{goalB} are propositions for two different goal regions.

Unless stated otherwise h_{enc} is a five layer network with size $\mathbb{R}^{n_x} \rightarrow 1024 \rightarrow 512 \rightarrow 256 \rightarrow 128 \rightarrow \mathbb{R}^{n_p}$ with a skip layer adding at the 512 layer and the base kernel used in the deep kernel models is the squared exponential (SE) kernel. When training we

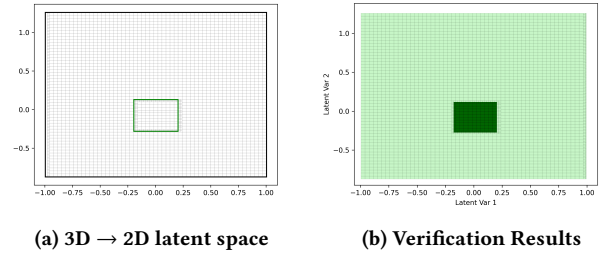


Figure 4: Results for “3D-Nonlinear-to-2D” Case Study. (a) The 2D latent space with the goal shown outlined in green, the domain outlined in black. (b) The set of states in the latent abstraction that can be guaranteed to reach the goal with the initial abstraction. The result verifies that all latent states reach the goal region and remain in the domain.

first normalize the domain X such that it is contained by the n_x -dimensional unit ball. Experiments were run on an Intel Core i7-12700K CPU at 3.60GHz with 32 GB of RAM. We show verification results in the latent space with the goal in dark green, Q_{yes} in light green, obstacles in black, $Q_?$ in yellow, and Q_{no} in red.

6.1 3D Nonlinear to 2D

We first consider a problem where all dimensions are relevant to the dynamics but we would still like to reduce the dimensionality to make abstraction more tractable. The dynamics are as follows:

$$\theta(a) = \frac{\pi}{7} \cos a \quad (17a)$$

$$\begin{bmatrix} x_{k+1}^{(1)} \\ x_{k+1}^{(2)} \\ x_{k+1}^{(3)} \end{bmatrix} = \begin{bmatrix} 0.7 \left(x_k^{(1)} \cos \theta(x_k^{(3)}) - x_k^{(2)} \sin \theta(x_k^{(3)}) \right) \\ 0.7 \left(x_k^{(1)} \sin \theta(x_k^{(3)}) + x_k^{(2)} \cos \theta(x_k^{(3)}) \right) \\ 0.7 x_k^{(3)} \end{bmatrix} \quad (17b)$$

In this example, the state $p_{\text{goal}} \in L(\mathbf{x})$ if $\|\mathbf{x}\|_\infty \leq 0.2$ and $p_{\text{unsafe}} \in L(\mathbf{x})$ if $\|\mathbf{x}\|_\infty > 1$. We also consider if we can make use of knowledge about the system to improve verification results and require that the encoder is learned such that the mapping for $x^{(1)}$ is identity. We emphasize that the 3D dynamics are the minimal realization for the system, and traditional techniques like PCA cannot identify a lower dimensional space without removing information.

We use 10000 data points to learn the encoder and the DKL model, and 1000 data points for prediction. The encoder is a five layer network with size $\mathbb{R}^{n_x} \rightarrow 512 \rightarrow 256 \rightarrow 128 \rightarrow 64 \rightarrow \mathbb{R}^{n_p}$ with a skip layer adding at the 256 layer. It takes less than 4 minutes to learn the encoder and the latent deep kernel from data, as well as map the regions of interest. We spend roughly 10 minutes to construct the transition function in the latent space and then less than 1 second is spent to verify against the specification.

The results for verification are shown in Figure 4. We note that the latent space is defined by a rectangle, as one dimension is mapped via an Identity transform and the other two dimensions are mapped through a convex function to a 1D output, each dimension of the latent space is independent of the others and defined over a convex range, which results in a rectangular latent space. We easily identify that the entire latent space satisfies our specification.

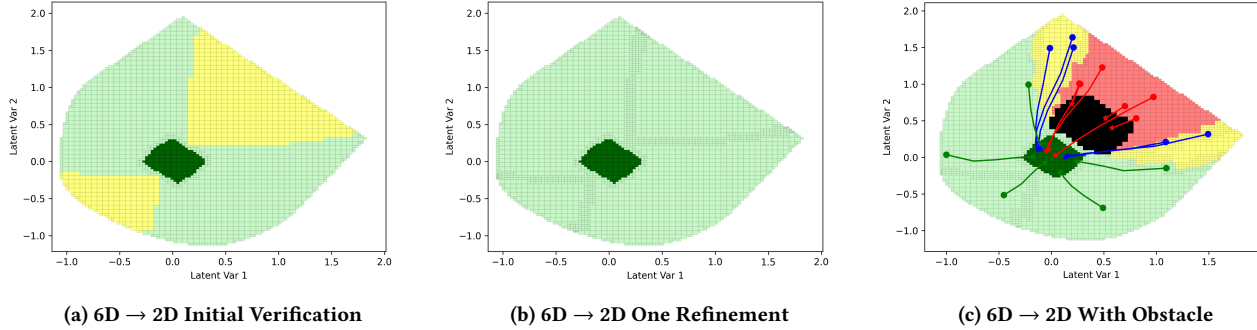


Figure 5: Verification results for the “6D-to-2D” case study. (a) the set of states in the latent abstraction that can be guaranteed to reach the goal with the initial abstraction, (b) after one refinement of the abstraction, and (c) with an obstacle. (c) We plot several trajectories (starting at circles and ending at stars) to verify result, green from Q_{yes} , blue from $Q_{?}$, and red from Q_{no} . When initializing in Q_{no} we find roughly 40% of trajectories collide with the obstacle and the remaining trajectories are safe and reach the goal. This conservatism comes from over-approximating the unsafe set in the latent space.

6.2 6D Nonlinear to 2D

With this example, we show that our approach can reason about over-parameterized models as well. We expand the dynamics of the previous example, and consider a state that includes observations of sin and cos terms, which results in the following dynamics:

$$\begin{bmatrix} x_{k+1}^{(1)} \\ x_{k+1}^{(2)} \\ x_{k+1}^{(3)} \\ x_{k+1}^{(4)} \\ x_{k+1}^{(5)} \\ x_{k+1}^{(6)} \end{bmatrix} = \begin{bmatrix} 0.7(x_k^{(1)}x_k^{(5)} - x_k^{(2)}x_k^{(6)}) \\ 0.7(x_k^{(1)}x_k^{(6)} + x_k^{(2)}x_k^{(5)}) \\ 0.7x_k^{(3)} \\ \cos 0.7x_k^{(3)} \\ \cos(\frac{\pi}{7} \cos(0.7 \cos^{-1}(x_k^{(4)}))) \\ \sin(\frac{\pi}{7} \cos(0.7 \cos^{-1}(x_k^{(4)}))) \end{bmatrix} \quad (18)$$

We make use of the same specification as before, where now $p_{goal} \in L(\mathbf{x})$ if $\|\mathbf{x}^{(1)}, \mathbf{x}^{(2)}, \mathbf{x}^{(3)}\|_\infty \leq 0.2$ and $p_{unsafe} \in L(\mathbf{x})$ if $\|\mathbf{x}\|_\infty \leq 1$. We use 15000 data points to learn the encoder, 10000 for the DKL model, and 1000 data points for prediction.

Results for verification are shown in Figure 5a-b. As in the last example, we identify that the entire latent space satisfies the specification. Figure 3 shows the Inclusion GP prediction from one point z^* in this latent space, where we generate the samples X'_{z^*} by decoding z^* with convex optimization.

We then consider a slightly more complex scenario, and introduce an obstacle to the environment defined as $o := \{\mathbf{x} | x^{(1)} \in [0.3, 0.6], x^{(2)} \in [-0.7, -0.3], x^{(3)} \in [-0.25, 0.25]\}$, then $p_{unsafe} \in L(\mathbf{x})$ if $\|\mathbf{x}\|_\infty > 1 \vee \mathbf{x} \in o$. Results for verification in this environment are shown in Figure 5c. We show trajectories in the latent space from Q_{yes} , $Q_{?}$, and Q_{no} . We note that since our method results in over-approximating unsafe regions we are conservative in identifying Q_{no} , which can be seen from trajectories that pass through the obstacle in the latent space but are safe in the high-dimensional space.

When mapping regions to the latent space, we make use of kinematic relations between the states. This knowledge is often easier to identify than the dynamics and does not require us to know

how the states evolve over time or which states define the minimal representation. This method helps reduce conservatism when over-approximating regions as our mapped points only contain kinematically feasible information.

6.3 26D to 2D, Reach-Avoid Specification

We demonstrate that our approach can be effective for systems that are high dimensional due to the control acting on high dimensional observations like LiDAR. We consider a system that must navigate around obstacles and reach a goal location where the controller is only given LiDAR-like observations and the direction to the goal position. For simplicity of presentation we consider a single integrator with 24 range readings at evenly spaced headings with a maximum range of 5 units. The controller is learned using PPO in a noisy environment.

We theorize that, given a set of obstacles and a goal position, a 2D latent space could be learned that models this system with minimal non-determinism. We use 10000 data points to learn the encoder, 30000 for the DKL model, and 1000 data points for prediction. It takes roughly 8 minutes to learn the encoder, 5 minutes to map the regions of interest (which is limited by the speed of the simulator), and 1 minute to learn the latent deep kernel. We spend roughly 12 minutes to construct the transition function in the latent space for the initial abstraction and one hour on 10 iterative refinements, with the majority of the time being spent on bounding the outputs of the Inclusion GP model. For each refinement less than 1 second is spent to verify the abstraction against the specification.

Figure 6 shows the 2D latent space and verification results we find with our method. We note that this space is visually similar to a flipped and scaled version of the original domain, but emphasize that LiDAR observations can strongly impact the point in the latent space. Our results verify that a significant volume of the latent space satisfies the specification, which corresponds to a significant portion of the original space being verified.

As the original function is not smooth (discontinuities in the LiDAR observations occur in domains that are non-convex due

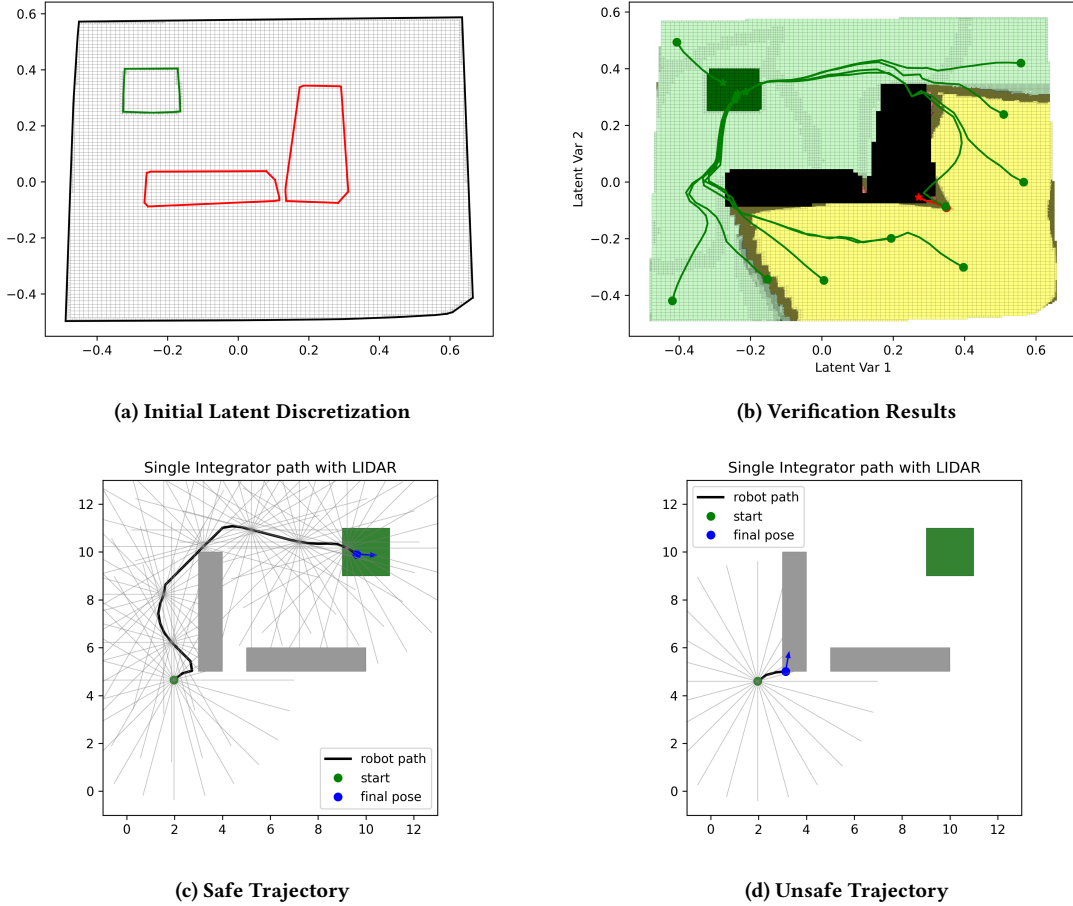


Figure 6: Results for the “26D-to-2D” case study. (a) The discretization and convex regions in the 2D latent space of the 26D system. (b) The verification results of the latent abstraction after 10 refinements. Multiple trajectories are plotted with green trajectories satisfying φ in the original space and red being unsafe. Note that many safe trajectories from the uncertain region exhibit unsafe behavior in the latent space. (c)-(d) The unsafe and safe latent trajectories that begin in the same region q from (b) shown in the original space of the system with LiDAR measurements shown every 5 time steps.

to obstacle placement), the function technically does not live in the RKHS of the SE kernel. We instead verify a set of continuous functions that capture the discontinuous evolution. This results in added conservatism in the abstraction, which can be seen with the unverifiable regions, the boundary of which corresponds to regions in the original space that have discontinuities in the dynamics. Alternate kernels that allow for discontinuities may improve the results. It is also possible that using local GP models for each region in which the dynamics are continuous would allow for a better abstraction as the system and approaches such as Work [20] could be used, but local GP regression is not explored in this work. We also stress that since the original system is discontinuous, it is impossible for a traditional neural network architecture to capture the evolution of the dynamics correctly (as common architectures can only model continuous systems), which further demonstrates the strength of our approach.

6.4 26D to 2D, Complex Specification

In this example we demonstrate that our approach can be used for infinite horizon guarantees and complex LTL specifications. We consider the same LiDAR system as in the previous example but in an environment with two goal locations and one obstacle. A memoryless controller is learned with PPO in a noisy environment. As the controller is memoryless, it is expected that only a small subset of the original space may satisfy the specification $\varphi = \square(\neg p_{\text{unsafe}}) \wedge \diamond(p_{\text{goalA}}) \wedge \diamond(p_{\text{goalB}})$ where p_{goalA} .

We use 10000 data points to learn the encoder, 30000 for the DKL model, and 1000 data points for prediction. It again takes roughly 8 minutes to learn the encoder, 4 minutes to map the regions of interest, and 1 minute to learn the latent deep kernel. After 5 iterative refinements of the latent abstraction, we identify the majority of the space where satisfaction is possible. The results are shown in Figure 7. We note that with a single obstacle, discontinuities in the

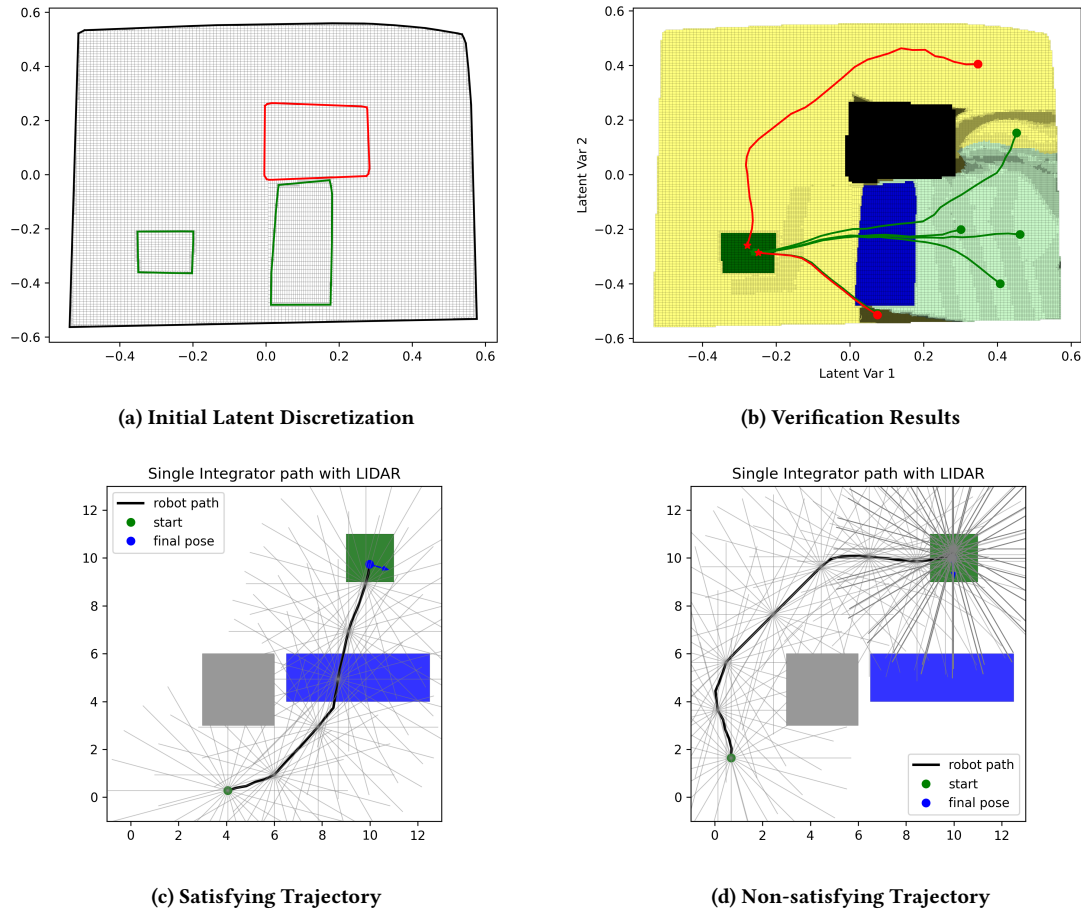


Figure 7: Results for the “26D-to-2D” two goal case study. (a) The discretization and convex regions in the 2D latent space of the 26D system. (b) The verification results of the latent abstraction after 5 refinements, with p_{goalA} in dark green and p_{goalB} in blue. Multiple trajectories are plotted with green trajectories satisfying φ in the original space and red not satisfying. Note that in the uncertain region below p_{goalB} there are both satisfying and non-satisfying trajectories. (c) An example satisfying trajectory that corresponds to the top most satisfying latent trajectory in (b) shown in the original space of the system with LiDAR measurements shown every 5 time steps, the trajectory is only plotted up to reaching both goals. (d) A non-satisfying trajectory in the original space that corresponds to the red trajectory starting in the top right in (b), the trajectory is plotted for 60 simulated seconds with much of that time spent circling in p_{goalA} .

dynamics from LiDAR measurements have a smaller impact on the abstraction than the previous example, allowing us to identify more of the satisfying space with our conservative, continuous model.

7 Conclusion

In this work we bridge a gap between dimensionality reduction and formal verification, defining a method that enables scalable abstraction-based verification for high dimensional systems with unknown dynamics. We reason about non-determinism in the latent space dynamics through a novel application of Gaussian Process Regression and demonstrate that a finite state abstraction can be correctly constructed in a latent space.

While our approach is sound, there are multiple aspects that limit the flexibility, namely restricting the encoder to be a convex function. While this restriction allows us to identify regions of interest in the latent space efficiently and correctly, it also limits the expressivity of the latent domain. Similarly there remain the open questions of how to accurately incorporate noise in the latent space and how to expand the method to control synthesis. We hope to address these limitations in future work

References

[1] Brandon Amos, Lei Xu, and J Zico Kolter. 2017. Input convex neural networks. In *International conference on machine learning*. PMLR, 146–155.

[2] Athanasios C Antoulas, Danny C Sorensen, and Serkan Gugercin. 2001. A survey of model reduction methods for large-scale systems. *Contemporary mathematics*, 280, 193–220.

[3] Asad Ullah Awan and Majid Zamani. 2025. Reduced-order gaussian processes for partially unknown nonlinear control systems. *IEEE Transactions on Automatic Control*.

[4] Christel Baier and Joost-Pieter Katoen. 2008. *Principles of model checking*. MIT press.

[5] Ulrike Baur, Peter Benner, and Lihong Feng. 2014. Model order reduction for linear and nonlinear systems: a system-theoretic perspective. *Archives of Computational Methods in Engineering*, 21, 4, 331–358.

[6] Calin Belta, Boyan Yordanov, and Ebru Aydin Gol. 2017. *Formal methods for discrete-time dynamical systems*. Vol. 89. Springer.

[7] Yoshua Bengio, Aaron Courville, and Pascal Vincent. 2013. Representation learning: a review and new perspectives. *IEEE transactions on pattern analysis and machine intelligence*, 35, 8, 1798–1828.

[8] Christopher M Bishop and Nasser M Nasrabadi. 2006. *Pattern recognition and machine learning*. Number 4. Vol. 4. Springer.

[9] Nathalia Cauchi, Luca Laurenti, Morteza Lahijanian, Alessandro Abate, Marta Kwiatkowska, and Luca Cardelli. 2019. Efficiency through uncertainty: scalable formal synthesis for stochastic hybrid systems. In *Proceedings of the 22nd ACM international conference on hybrid systems: computation and control*, 240–251.

[10] Xin Chen and Sriram Sankaranarayanan. 2016. Decomposed reachability analysis for nonlinear systems. In *2016 IEEE Real-Time Systems Symposium (RTSS)*. IEEE, 13–24.

[11] Sébastien Dalibard and Jean-Paul Laumond. 2011. Linear dimensionality reduction in random motion planning. *The International Journal of Robotics Research*, 30, 12, 1461–1476.

[12] Danijar Hafner, Timothy Lillicrap, Ian Fischer, Ruben Villegas, David Ha, Honglak Lee, and James Davidson. 2019. Learning latent dynamics for planning from pixels. In *International conference on machine learning*. PMLR, 2555–2565.

[13] K Lee, E Im, and K Cho. 2024. Mission-conditioned path planning with transformer variational autoencoder. *electronics* 2024, 13, 2437. *Advances in Human-Machine Interaction, Artificial Intelligence, and Robotics*, 164.

[14] Thomas Lew, Lucas Janson, Riccardo Bonalli, and Marco Pavone. 2022. A simple and efficient sampling-based algorithm for general reachability analysis. In *Learning for Dynamics and Control Conference*. PMLR, 1086–1099.

[15] Paul Lutkus, Kaiyuan Wang, Lars Lindemann, and Stephen Tu. 2025. Latent representations for control design with provable stability and safety guarantees. *arXiv preprint arXiv:2505.23210*.

[16] Daniele Masti and Alberto Bemporad. 2021. Learning nonlinear state-space models using autoencoders. *Automatica*, 129, 109666.

[17] Giulia C Matrone, Christian Cipriani, Emanuele L Secco, Giovanni Magenes, and Maria Chiara Carrozza. 2010. Principal components analysis based control of a multi-dof underactuated prosthetic hand. *Journal of neuroengineering and rehabilitation*, 7, 1, 16.

[18] Kensuke Nakamura, Lasse Peters, and Andrea Bajcsy. 2025. Generalizing safety beyond collision-avoidance via latent-space reachability analysis. *arXiv preprint arXiv:2502.00935*.

[19] Goro Obinata and Brian DO Anderson. 2012. *Model reduction for control system design*. Springer Science & Business Media.

[20] Chiwoo Park. 2022. Jump gaussian process model for estimating piecewise continuous regression functions. *Journal of Machine Learning Research*, 23, 278, 1–37.

[21] Pascal Poupart and Craig Boutilier. 2002. Value-directed compression of pomdps. *Advances in neural information processing systems*, 15.

[22] Carl Edward Rasmussen, Christopher KI Williams, et al. 2006. *Gaussian processes for machine learning*. Springer.

[23] Robert Reed, Luca Laurenti, and Morteza Lahijanian. 2025. Error bounds for gaussian process regression under bounded support noise with applications to safety certification. In *AAAI Conf. on Artificial Intelligence*.

[24] Robert Reed, Luca Laurenti, and Morteza Lahijanian. 2023. Promises of deep kernel learning for control synthesis. *IEEE Control Systems Letters*.

[25] Oliver Schön, Sofie Haesaert, and Sadegh Soudjani. 2025. Formal control for uncertain systems via contract-based probabilistic surrogates. In *International Conference on Quantitative Evaluation of Systems and Formal Modeling and Analysis of Timed Systems*. Springer, 62–82.

[26] Sarath Sivaprasad, Ankur Singh, Naresh Manwani, and Vineet Gandhi. 2021. The curious case of convex neural networks. In *Joint European Conference on Machine Learning and Knowledge Discovery in Databases*. Springer, 738–754.

[27] John Skovbekk, Luca Laurenti, Eric Frew, and Morteza Lahijanian. 2025. Formal verification of unknown dynamical systems via gaussian process regression. *IEEE Transactions on Automatic Control*.

[28] Ingo Steinwart. 2001. On the influence of the kernel on the consistency of support vector machines. *Journal of machine learning research*, 2, Nov, 67–93.

[29] Paulo Tabuada. 2009. *Verification and control of hybrid systems: a symbolic approach*. Springer Science & Business Media.

[30] Michalis Titsias and Neil D Lawrence. 2010. Bayesian gaussian process latent variable model. In *Proceedings of the thirteenth international conference on artificial intelligence and statistics*. JMLR Workshop and Conference Proceedings, 844–851.

[31] Ewerton R Vieira, Aravind Sivaramakrishnan, Sumanth Tangirala, Edgar Granados, Konstantin Mischaikow, and Kostas E Bekris. 2024. Morals: analysis of high-dimensional robot controllers via topological tools in a latent space. In *2024 IEEE International Conference on Robotics and Automation (ICRA)*. IEEE, 27–33.

[32] Shiqi Wang, Huan Zhang, Kaidi Xu, Xue Lin, Suman Jana, Cho-Jui Hsieh, and J Zico Kolter. 2021. Beta-CROWN: efficient bound propagation with per-neuron split constraints for complete and incomplete neural network verification. *Advances in Neural Information Processing Systems*, 34.

[33] Manuel Watter, Jost Springenberg, Joschka Boedecker, and Martin Riedmiller. 2015. Embed to control: a locally linear latent dynamics model for control from raw images. *Advances in neural information processing systems*, 28.

[34] Graham R Wood and BP Zhang. 1996. Estimation of the lipschitz constant of a function. *Journal of Global Optimization*, 8, 1, 91–103.

[35] Xiyue Zhang, Benjie Wang, Marta Kwiatkowska, and Huan Zhang. 2025. Premap: a unifying preimage approximation framework for neural networks. *Journal of Machine Learning Research*, 26, 133, 1–44.

A Appendix

A.1 Semantics of LTL and NNF

The semantics for an LTL specification are defined inductively as follows.

$$\begin{aligned}
 \omega_{x0} \models p &\iff p \in L(x_0) \\
 \omega_{x0} \models \neg\varphi &\iff \omega_{x0} \not\models \varphi \\
 \omega_{x0} \models \varphi \vee \psi &\iff \omega_{x0} \models \varphi \text{ or } \omega_{x0} \models \psi \\
 \omega_{x0} \models \varphi \wedge \psi &\iff \omega_{x0} \models \varphi \text{ and } \omega_{x0} \models \psi \\
 \omega_{x0} \models \bigcirc\varphi &\iff \omega_{x1} \models \varphi \\
 \omega_{x0} \models \varphi \mathcal{U} \psi &\iff \exists j \geq 0 \text{ s.t. } \omega_{xj} \models \psi \text{ and } \forall k < j \omega_{xk} \models \varphi \\
 \omega_{x0} \models \diamond\varphi &\iff \exists j \geq 0 \text{ s.t. } \omega_{xj} \models \varphi \\
 \omega_{x0} \models \square\varphi &\iff \forall j \geq 0 \omega_{xj} \models \varphi
 \end{aligned}$$

As noted, \square , \diamond , and \wedge can be defined using \neg , \mathcal{U} , and \vee , but to define Negation Normal Form (NNF), the semantics of \square , \diamond , and \wedge must be made clear.

Any LTL formula in NNF is defined inductively as

$$\begin{aligned}
 \text{NNF}(p) &= p \\
 \text{NNF}(\neg p) &= \neg p \\
 \text{NNF}(\varphi \vee \psi) &= \text{NNF}\varphi \vee \text{NNF}\psi \\
 \text{NNF}(\varphi \wedge \psi) &= \text{NNF}\varphi \wedge \text{NNF}\psi \\
 \text{NNF}(\neg(\varphi \vee \psi)) &= \text{NNF}(\neg\varphi \wedge \neg\psi) \\
 \text{NNF}(\neg(\varphi \wedge \psi)) &= \text{NNF}(\neg\varphi \vee \neg\psi) \\
 \text{NNF}(\bigcirc\varphi) &= \bigcirc\text{NNF}(\varphi) \\
 \text{NNF}(\neg \bigcirc \varphi) &= \bigcirc\text{NNF}(\neg\varphi) \\
 \text{NNF}(\varphi \mathcal{U} \psi) &= \text{NNF}(\varphi) \mathcal{U} \text{NNF}(\psi) \\
 \text{NNF}(\neg(\varphi \mathcal{U} \psi)) &= \text{NNF}(\neg\varphi) R \text{NNF}(\neg\psi) \\
 \text{NNF}(\diamond\varphi) &= \diamond\text{NNF}(\varphi) \\
 \text{NNF}(\neg \diamond \varphi) &= \square\text{NNF}(\neg\varphi) \\
 \text{NNF}(\square\varphi) &= \square\text{NNF}(\varphi) \\
 \text{NNF}(\neg \square \varphi) &= \diamond\text{NNF}(\neg\varphi)
 \end{aligned}$$

where R is the "release" operator defined as $\varphi R \psi \equiv \neg(\neg\varphi U \neg\psi)$.

Then if $\bar{\varphi}$ has no negations on any proposition, as it is defined over $p, p_n, \neg\bar{\varphi}$ will have negations on all propositions.

A.2 Proof of Lemma 1 (connected inclusion dynamics)

First we prove that an ICNN with the additional constraints listed in Section 4.1 will have connected pre-images.

The pre-image of a function f from a point y is the set $\{x \mid f(x) = y\} = f^{-1}(y)$. This set is referred to as a fiber. With an abuse of notation we use $(\cdot)^{-1}$ to denote the pre-image of a function (i.e. a non invertible matrix still has a well defined pre-image).

Let $A_1 : \mathbb{R}^n \rightarrow \mathbb{R}^t$ be an injective affine map (i.e. $t \geq n$), let $\phi : \mathbb{R}^t \rightarrow \mathbb{R}^t$ be a coordinate-wise strictly monotone, convex continuous map (hence a homeomorphism onto its image), let $A_2 : \mathbb{R}^t \rightarrow \mathbb{R}^m$ be an affine map whose linear part has full row rank m (so A_2 is surjective), and let $A_3 : \mathbb{R}^n \rightarrow \mathbb{R}^m$ be an injective affine map (i.e. $m \geq n$, hence $t \geq m \geq n$). Define

$$s(x) = A_2(\phi(A_1(x))) + A_3(x) \quad (19)$$

then, for every $y \in \mathbb{R}^m$ the fiber $s^{-1}(\{y\})$ is connected.

Let $s : \mathbb{R}^n \rightarrow \mathbb{R}^m$ be the encoder up to the first skip layer, we note that this defines a skip to layer two, but the argument holds for deeper skip layers under the same logic. Write $f(x) = A_2(\phi(A_1(x)))$ and $g(x) = A_3(x)$, then $s = f + g$. We prove two facts and then combine them.

First, every fiber of f is convex. Let $S := A_1(\mathbb{R}^n) \subset \mathbb{R}^t$. Since A_1 is injective and affine, S is an n -dimensional affine subspace of \mathbb{R}^t . As pre- and post- composing affine homeomorphism does not break the connectedness of fibers, we can assume without loss of generality that the affine subspace S is shifted through an affine transformation T to $\{(u_1, \dots, u_n, 0, \dots, 0)\}$ and then reason over this shifted coordinate space. Since ϕ is coordinate-wise strictly monotone, the mapping of the shifted subspace

$$\Phi := \phi|_{TS} : TS \rightarrow M := \phi(TS) \quad (20)$$

is also a homeomorphism from the affine subspace S onto the set $M \subset \mathbb{R}^t$. Thus M is homeomorphic to \mathbb{R}^n . Fix $y \in \mathbb{R}^m$, the fiber of f over y is

$$f^{-1}(\{y\}) = \{x \in \mathbb{R}^n : A_2(u) = y, u = \phi(A_1(x)) \in M\} \quad (21)$$

Equivalently

$$f^{-1}(\{y\}) = \{u \in M : A_2(u) = y\} = M \cap L_y \quad (22)$$

where $L_y := \{u \in \mathbb{R}^t : A_2(u) = y\}$ is an affine subspace of \mathbb{R}^t . Observe that M is the continuous image of the affine space TS under a coordinate-wise strictly monotone map, hence M is a convex set defined with intervals over the first n dimensions and constants for the next $t - n$ dimensions. The intersection of convex sets is convex and hence connected. Therefore f has connected pre-images.

Now we consider adding an injective affine map and show that this preserves connected fibers. Fix $y \in \mathbb{R}^m$, the fiber of s over y is

$$s^{-1}(\{y\}) = \{x : f(x) + g(x) = y\} = \{x : f(x) = y - g(x)\} \quad (23)$$

The injectivity of g implies that g is a homeomorphism onto its image (S_3 an n -dimensional affine subspace of \mathbb{R}^m). Since g is an affine homeomorphism onto S_3 , $x = A_3^{-1}(u)$ for $u \in S_3$. We define a new function

$$\tilde{f}(u) := f(A_3^{-1}(u)) \text{ for } u \in S_3 \quad (24)$$

Since A_3^{-1} is a homeomorphism and every fiber of f is connected, every fiber of \tilde{f} is connected. Then the fiber condition for s becomes $\tilde{f}(u) + u = y$. Hence,

$$s^{-1}(\{y\}) = A_3^{-1}(\{u \in S_3 : \tilde{f}(u) + u = y\}) \quad (25)$$

Again since g is an affine homeomorphism, connected sets in S_3 correspond bijectively to connected sets in \mathbb{R}^n . Hence, the solution set to $\tilde{f}(u) + u = y$ is the continuous pre-image of a convex intersection as before and hence connected.

We note that $s(x)$ defines an ICNN with a skip layer after the first activation. Hence, by induction, all skip layers have connected pre-images. Continuity of the system enforces that the pre-image of a connected set in the affine subspace will be defined by the union of convex sets, which may be non-convex in general but will still be connected.

We can now consider the network after skip layers. Let $T : \mathbb{R}^k \rightarrow \mathbb{R}^p$ be the final layers of the network where $k \geq n \geq p$ as the last skip layer must remain injective. T is composed of monotone, full rank, affine transformations that reduce dimensionality and strictly monotone non-linear activations. Each affine transformation, by definition, has a connected pre-image. Strictly monotone non-linear activations are homeomorphism, and hence also have connected pre-images. Therefore T has a connected pre-image for any point. Following arguments from s , the pre-image of T under a point will be a convex set. The intersection of a convex set with an affine subspace will be a connected set in the affine subspace, hence the entire network is guaranteed to have a connected pre-image from a point, resulting in a CICO network.

Then, by Lemma 1, \mathcal{X}_z is a connected set. Further, by continuity of f , \mathcal{X}'_z is also connected. The continuity of h_{enc} then ensures connectivity of \mathcal{Z}' .

A simple condition to check is if the Jacobian of the network has rank n_p . If this is satisfied, along with the architectural constraints, then the fibers are connected as the network is a proper submersion.

A.3 Proof of Lemma 2 (Conservative Labeling)

Recall Z defines an under-approximation of domain X in the latent space. Also recall that Eq. (9b) defines a high confidence over-approximation in the latent space for region r_i by Proposition 2, that is $r_{\hat{Z},i}$ defines a convex set in the latent space that will contain all points $\{h_{enc}x \mid x \in r_i\}$ with high confidence, therefore $Z \setminus r_{\hat{Z},i}$ is an under-approximation of $X \setminus r_i$ in the latent domain Z . Also recall that in the original space $p_{n,i} \in L(x \in X \setminus r_i)$, then by labeling $Z \setminus r_{\hat{Z},i}$ with $p_{n,i}$ we under-approximate the label in the latent space. The logic follows similarly for labels p_i , as we first over-approximate $X \setminus r_i$ in the latent space. This implies that if $p_i \in L(q_x)$ then $p_i \in L(x)$ for $h_{enc}(x) \in q_x$, hence $L(q_x) \subseteq L(x)$.

A.4 Proof of Lemma 3

With CICO h_{enc} and continuous f, g is Hausdorff continuous, intuitively if z_0 is close to z_1 then every point in $g(z_0)$ is close to a point in $g(z_1)$. Since the set $g(z)$ is path connected and compact, there exists a continuous surjection $\gamma_z : [a, b] \rightarrow g(z) \subseteq \mathbb{R}^{n_p}$. The continuity of g implies that the surjection γ_z also varies continuously with z . We define the total continuous function $G : \mathbb{R}^{n_p} \times [a, b] \rightarrow \mathbb{R}^{n_p}$ as $G(z, c) = \gamma_z(c)$. By fixing a parameter $c \in [a, b]$ the resulting map

$g_c(z) = G(z, c)$ is continuous from \mathbb{R}^{n_p} to \mathbb{R}^{n_p} and the continuous family $\{g_c \mid c \in [a, b]\}$ defines the image of g .

A.5 Proof of Theorem 3 (Sound Abstraction)

By Lemma 2, $L(q) \subseteq L(x)$ for $(x, q) \in \mathcal{R}$. By Proposition 3, for every transition $x' = f(x)$ if $(x, q) \in \mathcal{R}$ then $\exists q'$ such that $T(q, q') = 1$ and $(x', q') \in \mathcal{R}$. This satisfies the requirements for a sound abstraction.

We then prove the contrapositive,

$$\omega_{x_0} \not\models \bar{\varphi} \implies \exists \omega_{q_0} \not\models \bar{\varphi}$$

That is, any counter example on System (1) must also have a counter example in the NTS. A sound abstraction ensures $\exists \omega_{q_0}$ that remains in relation with ω_{x_0} for all $i \geq 0$. Recall that $\bar{\varphi}$ has no negations at all, so $\neg \bar{\varphi}$ can be written in NNF where negations are applied to all propositions.

Assume $\omega_{x_0} \not\models \bar{\varphi}$, i.e. $\omega_{x_0} \models \neg \bar{\varphi}$. We begin with the base case $\bar{\varphi} := p$. Then $\omega_{x_0} \not\models p$ means $p \notin L(x_0)$ and since $L(q_i) \subseteq L(x_i)$ this implies $p \notin L(q_0)$ and therefore $\omega_{q_0} \models \neg p$. Hence satisfaction of negative propositions in AP is preserved from System (1) to N. Since ω_{q_0} remains in relation with ω_{x_0} , the satisfaction of negated propositions holds at subsequent states. By the semantics of LTL this satisfaction is applied inductively to Boolean and Temporal Operators. Then $\omega_{x_0} \not\models \bar{\varphi}$ implies $\exists \omega_{q_0} \not\models \bar{\varphi}$. This establishes the contrapositive and hence $\Omega_q \models \bar{\varphi} \implies \omega_x \models \bar{\varphi}$.